Urban Climate 47 (2023) 101384

Contents lists available at ScienceDirect

Urban Climate

journal homepage: www.elsevier.com/locate/uclim

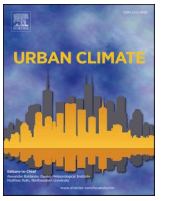

# Air pollution in central European capital (Budapest) via self-made passive samplers and Sentinel-3B SYN satellite images

Alcindo Neckel [a,*], Marcos L.S. Oliveira [b,c], Laércio Stolfo Maculan [a], Brian William Bodah [a,d,e], Affonso Celso Gonçalves Jr [f], Luis F.O. Silva [b,*]

[a] ATITUS Educação, 304- Passo Fundo, RS 99070-220, Brazil
[b] Department of Civil and Environmental Engineering, Universidad de la Costa, CUC, Calle 58 # 55–66, Barranquilla, Atlántico, Colombia
[c] Department of Sanitary and Environmental Engineering, Federal University of Santa Catarina - UFSC, 88040-900 Florianópolis, Brazil
[d] Thaines and Bodah Center for Education and Development, 840 South Meadowlark Lane, Othello, WA 99344, USA
[e] Yakima Valley College, Workforce Education & Applied Baccalaureate Programs, South16th Avenue & Nob Hill Boulevard, Yakima, WA 98902, USA
[f] Center for Medical and Pharmaceutical Sciences, State University of Western Paraná – UNIOESTE, Campus Cascavel, PR 85819-110, Brazil

ARTICLE INFO

*Keywords:*
Dispersion of pollutants
Global scale
Ultra-fine particles
Historical heritage
Population health

ABSTRACT

This study is to identify the types of ultra-fine air pollutants present in the local atmosphere. The authors utilize Sentinel-3B SYN satellite images to identify the presence of Aerosol Optical Thickness (T550), and later verify this presence through physical sample collection using self-made passive samplers (SMPSs) at various locations in Budapest ((A) Passenger Cruise Port, (B) Kunsthalle, (C) Szechenyi Lanchid, and (D) Liberty Bridge). The samples obtained from the SMPSs were analyzed by X-ray Diffraction (XRD) to identify the minerals present in ultra-fine phases (e.g. minerals and ultra-fine amorphous). The images from the Sentinel-3B SYN satellite, taken between 2018, 2019 and 2021 allowed us to identify the Aerosol Optical Thickness (T550) at these same locations in Budapest. The SMPS samples revealed the presence of ultra-fine particles containing elements dangerous to human health, such as: As, Cd, Cr, Hg, Pb, Ti, V and Ni. The points analyzed in the Sentinel-3B SYN satellite images showed a 50.89% reduction in T550 levels in the city of Budapest, attributed to the COVID-19 epidemic, which clearly demonstrates the need to reduce pollutants for a better quality of life in this central capital of Europe.

## 1. Introduction

Atmospheric pollution resulting from the combination of industrial activities and motor vehicle traffic has become a complex problem in large cities worldwide in recent decades, compromising environmental quality due to the high diversity of hazardous elements released into the atmosphere in the form of gases. Such gases include $CO_2$ (carbon dioxide), $N_2O$ (nitrous oxide), $CH_4$ (methane) and $O_3$ (ozone). Additionally, aggregates of nanometric and ultra-fine particles, which are harmful to human health, also often raise the temperature of cities, exacerbating the heat island effect (Islam et al., 2020; Forest, 2021). Fossil emissions of $CO_2$ are driven mainly through the combustion of oil and coal, leading to anthropogenic climate change on a global level (Li et al., 2021). $N_2O$ is generated through decomposition by microorganisms present in the soil in addition to the production and use of chemical fertilizers

* Corresponding authors.
*E-mail addresses:* alcindo.neckel@atitus.edu.br (A. Neckel), lsilva8@cuc.edu.co (L.F.O. Silva).

https://doi.org/10.1016/j.uclim.2022.101384
Received 24 May 2022; Received in revised form 14 November 2022; Accepted 9 December 2022
Available online 19 December 2022

for agricultural use, and the burning of biomass and fossil fuels (Kong et al., 2020; Addington et al., 2021). Anthropogenic emissions of $CH_4$ are driven mainly by landfilling operations, plantations, followed by mining activities and forest fires (the majority of which are human caused) (Pirmana et al., 2021). $O_3$ is a gas often formed from $NO_x$ (nitrogen oxides) and hydrocarbons, released in the form of nanoparticles and ultra-fine particles with atmospheric contaminants (whether organic or inorganic). $O_3$ is released in large quantities by thermoelectric power plants and the internal combustion engines of motor vehicles, thus raising levels of atmospheric contamination on a global scale (Dong et al., 2021; Forest, 2021).

Several gases can react once in the atmosphere to form particles smaller than 50 nm (Li et al., 2020; Nassajpour-Esfahani et al., 2021). Such particles can remain suspended in the atmosphere for long periods of time. Once these particles aggregate with dust particles, containing different structures, they present a great risk to the population (Bao et al., 2022; Zhang et al., 2022). These pollutants present in the air are also capable of accelerating the degradation of historic buildings listed by the United Nations Educational, Scientific and Cultural Organization (UNESCO). Such historic sites preserve the heritage of humanity.

For better detection of atmospheric contaminants, the European Space Agency (ESA) makes available Sentinel-3B SYN satellite images to registered and trained researchers for the assessment of Aerosol Optical Thickness (T550) levels worldwide (Fernandez-Moran et al., 2021). Aerosol Optical Thickness analysis consists of the technical application of remote sensing aimed at detecting aerosols using the Radiative Transfer Model (RTM). The high precision of the RTM allows for identification of aerosols suspended over the ground level (Mei et al., 2020).

Aerosols are compounds capable of containing high loads of atmospheric contaminants that spread over large regions, absorbing solar radiation, and leading to a greater imbalance in temperature in cities around the world (Mei et al., 2020; Fernandez-Moran et al., 2021; Bodah et al., 2022). One of these cities, Budapest, which is the ninth largest city in Europe, can be related to other European cities where studies have identified high concentrations of particulate materials and gases harmful to human health and historic buildings (Kovács et al., 2021; Silva et al., 2022). Kovács et al. (2021) studied atmospheric pollution in the urban area of Budapest and identified high levels of dispersion of atmospheric pollutants based on a geospatial grid of 1 km × 1 km using the Global Forecast

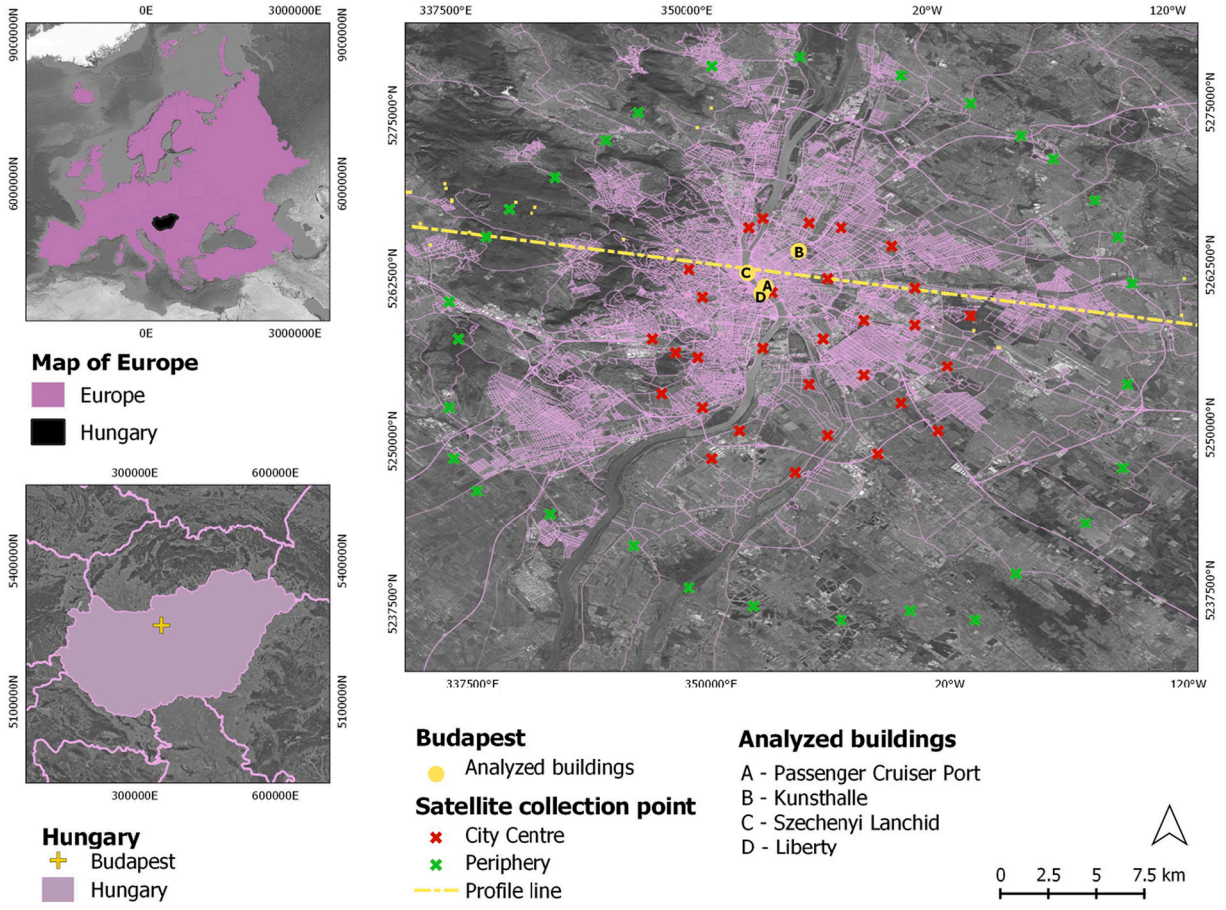


**Fig. 1.** Map showing the location of the city of Budapest, capital of Hungary (Europe). Also shown is the location of the following historic buildings and monuments: (A) Passenger Cruise Port, (B) Kunsthalle, (C) Szechenyi Lanchid and (D) Liberty Bridge. Field samples were collected at sites A, B, C and D, as each had high rates of tourist traffic. Also shown is the points collected from the images of the S3B SYN Satellite. Source: Modeling from the ESA database (2022).

System (GFS) in both winter and summer of 2016. Their results yielded average values of atmospheric emission levels of CO = 11.1, $NO_x$ = 9.3 and $O_3$ = 1.8 t/day. This could be associated with an average of 8000 annual deaths related to air pollution in Hungary, aggravated by the emission of gases released by industrial activities and those derived from the burning of fossil fuels by motor vehicles (Kovács et al., 2021).

According to the International Association for Medical Assistance to Travelers (IAMAT, 2022) the air quality in Budapest, Hungary is harmful to human health as it has an annual average concentration of $PM_{2.5}$ of 16 μg/m$^3$, thus exceeding the maximum recommended limits of 10 μg/m$^3$, set by the World Health Organization (WHO). For Buzási et al. (2021) the city of Budapest needs to establish urgent environmental sustainability strategies aimed at improving air quality. Doing so would not only improve local air quality but also contribute to the mitigation of climate change on a global scale. They also highlight the need to carry out more studies that make it possible to identify the types of contaminants in ultra-thin thicknesses, with the degree of expansion of hazardous elements suspended in the atmosphere. Further investigation yielding more specific results may facilitate the creation of possible mitigating solutions for the emissions of atmospheric gases harmful to human health (Buzási et al., 2021). Human health is not the only thing that can be harmed by poor air quality as atmospheric pollutants can negatively impact the quality of historic buildings as well (Morillas et al., 2018; García-Florentino et al., 2020; Oliveira et al., 2021; Silva et al., 2022). This particular manuscript examines the buildings and monuments of Budapest, listed by UNESCO as World Heritage Sites.

The general objective of this study is to identify the types of ultra-fine air pollutants present in the local atmosphere. The authors utilize Sentinel-3B SYN satellite images to identify the presence of Aerosol Optical Thickness (T550), and later verify this presence through physical sample collection using self-made passive samplers (SMPSs) at various locations in Budapest.

## 2. Material and methods

### 2.1. Study area

The city of Budapest is the capital of Hungary located in Eastern Europe (Fig. 1). The city center of Budapest is formed by the region of Pest (plain), demarcated by the main avenue Nagykörút, serving as the main center of business, banks and commerce. Hungary has enjoyed a consistent rise in tourism and touristic activities due to the conservation of buildings and historical monuments (Dövényi et al., 2021; Kovács et al., 2021). The urban area of Budapest is divided by the Danube River, but has been united through the construction of bridges and other infrastructure since before the First World War (Kovács et al., 2019). Kovács et al. (2019) highlight that many of Budapest's historic buildings have deteriorated severely due to the lack of application of projects aimed at their conservation. This cultural heritage is characterized by the diversity of architectural styles from different times, ranging from this the influence of the ancient Roman City of Aquincum in Óbuda from 89 CE, to Gothic and Renaissance architecture. Beginning in 1990, urban rehabilitation interventions with the goal of restoration and maintenance projects of historic buildings in Budapest commenced in the central


**Fig. 2.** Historic buildings and monuments analyzed in the city center of Budapest: (A) Passenger Cruise Port, (B) Kunsthalle, (C) Szechenyi Lanchid and (D) Liberty Bridge.

region (Kovács et al., 2019).

The city of Budapest in 2021 has an estimated population of 9,992,662 inhabitants, and comprises a territory of 93.032 $km^2$, with a density of 107.4 inhab/$km^2$ (Dövényi et al., 2021). Regarding the climate, Budapest has warm summers and cold winters, with extensive layers of snow and a sky partially covered by clouds, where average annual temperatures vary from −3 °C in winter to 27 °C in summer (Dövényi et al., 2021). In this context, there is a need to study the impacts of atmospheric pollution, identifying chemical elements that contribute to the corrosion of historical buildings and the resulting impacts on human health. This was completed through samples collected in the field in the following historic buildings and monuments in Budapest's city center: (A) Passenger Cruise Port, (B) Kunsthalle, (C) Szechenyi Lanchid, and (D) the Liberty Bridge (Fig. 2). These sites were selected because of their high historical and cultural importance, leading to the high number of visitors and tourists who visit annually. Studies involving atmospheric contamination related to the degradation of historical and cultural heritage should consider the places in a given area with the highest overall number of tourist visits. These locations experience the greatest circulation of individuals who may be exposed to the microparticles housed in these buildings and historic monuments (Silva et al., 2022). Neckel et al. (2021) and Li et al. (2022) attribute the importance of studies using satellite images, as the most complete method to analyze the presence and variation of particulate contaminants on macroscales in high resolution.

### 2.2. Particulate material collection procedures and sample analysis

In order to obtain reliable results related to the presence of ultra-fine particles, three SMPSs were installed on poles during the four seasons of 2018. The samplers were located within a radius of up to 50 m from the buildings and monuments (Fig. 2 A, B, C and D), at a height between 1.3 m and 1.5 m from ground level, as this is considered the variation of mean human respiratory height (Oliveira et al., 2021; Silva et al., 2022). The buildings and monuments selected in this study have a high circulation of both local inhabitants. The (A) Passenger Cruise Port consists of the main boat station in Budapest, serving as a meeting place and busy passage of residents and tourists. Characterized as a port, it receives people for arrival and departure on navigable transfers along the Danube River and its tributaries (Buzási et al., 2021; Buzási, 2022). (B) The Kunsthalle is Budapest's museum of contemporary art. A historic building of Green Renaissance and neoclassical architectural style, it was built in 1896. The Kunsthalle underwent restoration in 1995, receiving improvements which allows it to receive a greater number of tourists (Buzási et al., 2021). (C) The Szechenyi Lanchid is a historic bridge connecting Buda and Pest, officially inaugurated in 1849 to carry pedestrian traffic in addition to the vehicles of that era. It is one of the greatest symbols of Budapest (Buzási, 2022). (D) Liberty Bridge, built of cast iron in 1896 measures 330 m in length and was constructed in the Art Nouveau style. It contains in its structure mythological sculptures located in its towers, that are related to the culture of Budapest (Buzási et al., 2021; Buzási, 2022). Accumulations and reactions of particulate chemical elements were visible, forming black crusts (Morillas et al., 2018; García-Florentino et al., 2020) in structures B and C (Fig. 2).

In calendar years 2018 and 2019, 48 samples were collected via SMPS to determine the concentration of ultra-fine materials present

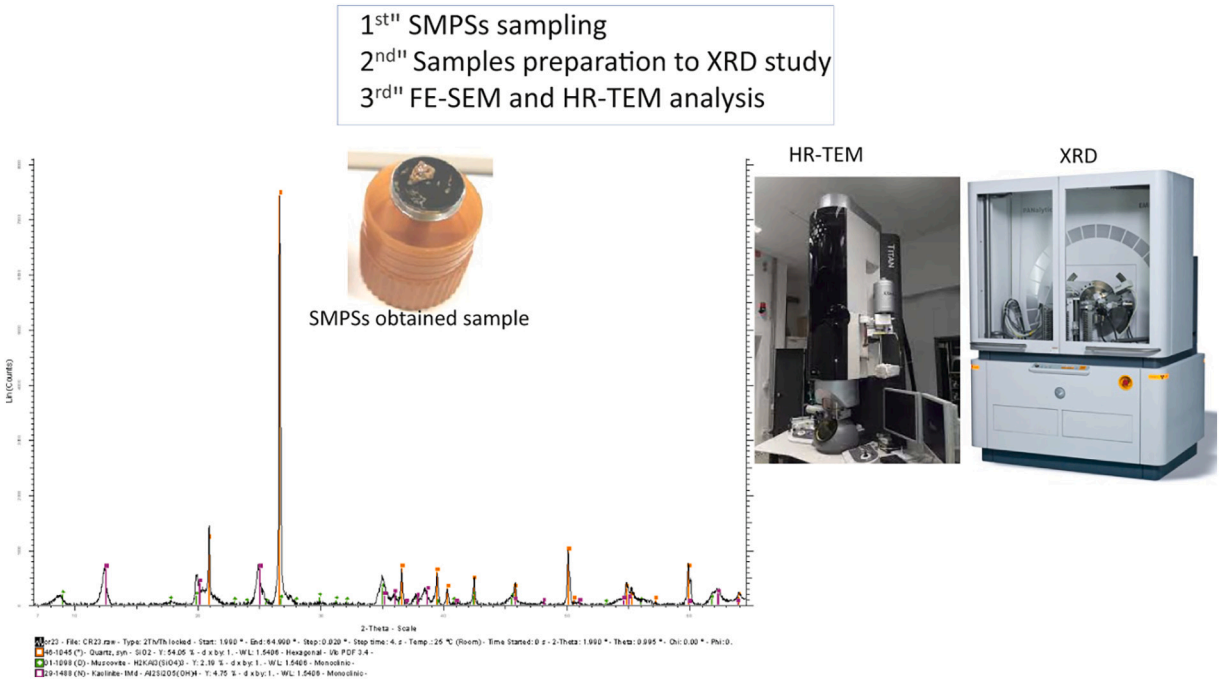


**Fig. 3.** Representation of the equipment used in this study: (1st) SMPS sampling, (2nd) sample preparation for XRD study and (3rd) FE-SEM and HR-TEM analysis, with identification of the most abundant phases detected by XRD.

in the local atmosphere SMPSs were emptied quarterly, on December 9, 2018, March 25, 2019, June 7, 2019, and September 25, 2019; and a new collection surface was placed in each SMPS for later collection at each of the buildings and historic monuments A, B, C and D (Fig. 2). After collection, the samples were isolated in sterilized glass containers to avoid contamination from external elements, until they were sent to the Environmental Chemistry Laboratory of the Universidad de La Costa – CUC, located in the city of Barranquilla, Colombia. In the laboratory, the samples were prepared in triplicate and initially analyzed by X-ray Diffraction (XRD) as it is a non-destructive and effective technique to detect minerals (Fig. 3). Subsequently, the samples were analyzed by Field Emission Scanning Electron Microscopy (FE-SEM) to understand the formation of ultra-fine particles; and finally, by High Resolution Transmission Electron Microscopy HR-TEM, according to Morillas et al. (2018), García-Florentino et al. (2020), Oliveira et al. (2021), Pinto et al. (2021) and Silva et al. (2022) so that the nanoparticles present in the area under study could also be evaluated. Through this analyzed particulate matter, it became possible to understand the most abundant minerals, as well as the minority phases, whether mineral and/or amorphous (Morillas et al., 2018; Pinto et al., 2021; Silva et al., 2022).

This study highlights the importance of detecting particles smaller than 0.1 μm (e.g. soot particles) not yet studied in detail in the city of Budapest. This study contributes to the important task of knowing the chemical, mineralogical and morphological makeup of the most abundant particles; whether amorphous or minerals, smaller than 0.1 μm, as they have a greater harmful impact on human health (Gasparotto et al., 2018; Oliveira et al., 2021; Silva et al., 2022), in addition to contributing to the degradation of structures of historical buildings and monuments (Morillas et al., 2018; García-Florentino et al., 2020; Oliveira et al., 2021). The efficiency of results obtained through the use of SMPSs has been demonstrated in studies by Morillas et al. (2018), Oliveira et al. (2021) and Silva et al. (2022) in relation to the identification of ultrafine particles in urban environments. However, when these data are compared with satellite imagery obtained from the same area, it becomes possible to understand and extrapolate the movement of concentrations of atmospheric pollutants (Bodah et al., 2022; García and Díaz, 2022). This greatly enhances the relevance of this study for the city of Budapest.

### 2.3. Sentinel-3B SYN procedures for detection of air pollutants

The use of images from the Sentinel-3B SYN satellite, at level 2 (SYN), responsible for providing daily global images with a spatial resolution of 260 m is under the domain of the Center of the European Space Agency (ESA). This allowed the authors to carry out retrospective analyses. In this study, satellite images of Budapest were acquired during all four seasons (winter, spring, summer and autumn) for the years 2018, 2019 and 2021 (Table 1). Only a single image obtained in 2018 from the Sentinel-3B SYN satellite was used. This was due to excess cloud cover over the city of Budapest in available 2018 images. Satellite imagery remains a very versatile tool, but one that is vulnerable to natural cloud cover. Sentinel-3B SYN satellite images obtained during collection periods at points A, B, C and D (Fig. 2) in 2018 and 2019 were utilized for the central region of Budapest. The choice of performing space sampling in 2021 made it possible to work with unpublished images from the Sentinel-3B SYN satellite provided by the ESA (2022). Thus, considering the recommendation by Neckel et al. (2021), who suggested the need for more studies at a global level with the use of satellite images, considering the current pandemic scenarios caused by COVID-19.

Processing of the Sentinel-3B SYN satellite images was performed using the SNAP software version 8.0.4. based on advanced technology of commands assigned to the Geographic Information System (GIS), for the evaluation of the Aerosol Optical Thickness variable (T550), also assigned to the altimetry item (Alt) (ESA, 2022). The T550 concentration considers the existing aerosol charge, expressed in optical thickness, with a wavelength of 550 nm, with estimates of the associated error reduction. Alt considers the satellite collection points positioned as follows: 30 points in Budapest's city center and 30 points in its periphery.

To verify the related concentration of T550 to Alt in the city of Budapest, the statistical similarity in k-means clusters was analyzed through a set of information gathered and organized in a single database. These data originated from the results of the collections carried out between the points sampled in the Sentinel-3B SYN satellite images, containing the variation of the air pollutant patch. Subsequently, the analysis of the database was performed using the JASP statistical software version 0.14.1.0. (Ngah Nasaruddin et al., 2021). K-means groupings were performed starting with Eq. (1), containing the representation of (d) distance between points, (pi) point of a cluster, (x{x1, xk}) elements, and (n) number of elements (Dal Moro et al., 2021). Sequentially, Eq. (2), based on (SSE) sum

**Table 1**
Dates and acquisition of Sentinel-3B SYN satellite images.

| 2021 | Image Date (Sentinel-3B SYN) | Denomintion |
|---|---|---|
| Winter | March 1, 2021 | Win 2021 |
| Spring | May 10, 2021 | Spr 2021 |
| Summer | August 10, 2021 | Sum 2021 |
| Autumn | October 25, 2021 | Aut 2021 |

| 2018/2019 | Image Date | Denomination |
|---|---|---|
| Winter | February 28, 2019 | Win2019 |
| Spring | March 31, 2019 | Spr2019 |
| Summer | July 1, 2019 | Sum2019 |
| Autumn | October 8, 2018 | Aut2018 |

of squares of errors, (Ni) total elements, (Xij) elements, and (Ci) centroid point, to finally apply Eq. (3), considering (S(i)) average of all data in the group, (b(i)) minimum distance of data i to all other data that does not belong to your group, and (a(i)) average distance of data "i" to all other data in your group, which made it possible to carry out optimization procedures, with data vectors, thus forming the clusters (Dal Moro et al., 2021).

$$d(p,x) = \frac{1}{n}\sum_{i=1}^{n} d(p_i,x)^2 \tag{1}$$

$$SSE2 = \frac{N_i \Sigma_j \left\| x_{ij} - c_i \right\| 2}{N_i - 1} < SSE1 = \frac{N_1 \Sigma_j \left\| x_{1j} - c_1 \right\| 2}{N_1 - 1} \tag{2}$$

$$S(i) = \frac{b(i) - a(i)}{max(a(i), b(i))} \tag{3}$$

The clusters originated in this study enabled the formation of the Silhouette index, which shows the average internal consistency of the group being evaluated, with a degree of similarity between clusters (Tardioli et al., 2018; Naghizadeh and Metaxas, 2020). For Silhouette scores, the closer you are to the upper bound of 1, the more consistent the data clustering becomes (Naghizadeh and Metaxas, 2020). However, when Silhouette scores approach the lower limit of −1 it may indicate an inaccurate correlation of the sampled data (Tardioli et al., 2018; Naghizadeh and Metaxas, 2020). Thus, facilitating a better understanding of the visualization of the expansion of atmospheric contamination in the city of Budapest, through the data collected in the Sentinel-3B SYN satellite images, also represented in specific clusters.

## 3. Results and discussion

### 3.1. Identification of particulate materials collected in SMPSs

The analyses carried out on the particulate materials, in the 48 samples obtained by SMPSs, between points A, B, C and D (Figs. 1 and 2) showed amorphous phases in most of the material collected. Although it was possible to identify several minerals, with the following order of abundance: quartz, albite, dolomite, calcite, muscovite, and gypsum (Table 2) detected by XRD (Fig. 3). Several other minerals were detected in smaller proportions (e.g. chlorite and illite), in addition to many fine particles, such as barite (Fig. 4 A), and nanometers, such as: anatase, rutile, hematite, magnetite, and mullite, detected by FE-SEM and HR-TEM. When related to the studies by Dai et al. (2021), who identified several ultra-fine and nanometric minerals, with phases present in coal and coal ash from Bulgaria, it is assumed that emissions from Bulgarian coal power plants have a strong influence on the air quality of Budapest. Several spherical amorphous phases identified in this study (Fig. 4 B), present similarities with the particles of coal fly ash. Consequently, there is an alert for the excessive use of coal in Hungary and its neighboring countries, based on studies that point to a probable degradation of respiratory quality in places where coal power plants are present (Gasparotto et al., 2018; Dai et al., 2021).

Regarding particles likely sourced from coal power plants, soil suspension is one of the biggest factors that contribute most of the particles detected with mineral content such as quartz, clays and several oxides. Such particles mostly had sizes >5 μm. It should be noted that in the port region, both large ships (which utilize fuels with high proportions of S) and medium and small ships have a direct impact on people's health (tourists and those who work and live around the port areas). Additionally, decay of construction materials utilized in local buildings can contribute to poorer air quality as pointed out in studies by Morillas et al. (2018), Oliveira et al. (2021) and Silva et al. (2022). In this case, the particles detected were much smaller than 0.1 μm, which greatly increases the potential negative impact on human health. Particles of this size, when inhaled, can easily enter the bloodstream through the lungs, causing measurable damage to human health (Morillas et al., 2018; Silva et al., 2022).

Murukutti and Jena (2022) show, when studying the mineralogical formation of ultra-fine particles and nanoparticles present in coal ash from different countries, the presence of minerals such as mullite and magnetite. Table 2 shows that coal power plants have a direct effect on air quality in Budapest as the samples obtained by the SMPSs contain several minerals and amorphous phases similar to coal fly ash. Furthermore, the presence of titanium (Ti), vanadium (V) and nickel (Ni) in mullite particles is due to chemical elements associated with some clays and mineralogical phases present in coal. Ti, V and Ni increase the toxicological risks to human health due to the high concentration of ultra-fine particles suspended in the air (Gasparotto et al., 2018; Aarzoo and Samim, 2022). According to Sánchez et al. (2011), Morillas et al. (2018) and Marvila et al. (2020), calcite, gypsum and quartz can be derived from the wear of construction materials, considering more accentuated processes in historic buildings. Therefore, the lack of maintenance of buildings,

**Table 2**
Main hazardous elements detected in the organic nanoparticles of the samples collected.

| Studied Area | Principal Hazardous Elements | Dimensional characteristics | |
|---|---|---|---|
| | | Diameter (nm) | Length (μm) |
| **A** | Ag, Ba, C, Cd, Cl, Co, Cr, Hg, Ge, Mn, Mg, Mo, Ni, Pb, Sb, Se, Sn, Sr, Ti, V, W, Zn, Zr | 48 ± 7 | 86 ± 9 |
| **B** | As, Ba, C, Cd, Cr, Cu, Hg, Mo, Ni, Sb, Sr, V, Zn, Zr | 92 ± 5 | 93 ± 3 |
| **C** | As, Ba, C, Cu, Cl, Co, Hg, Mn, Mo, Ni, Sb, Se, Sn, Ti, Zn, Zr | 73 ± 1 | 104 ± 5 |
| **D** | Ag, As, Ba, C, Cd, Co, Cu, Hg, Mo, Ni, Pb, Sb, Se, Sn, Sr, Ti, W, V, Zn | 51 ± 3 | 95 ± 7 |

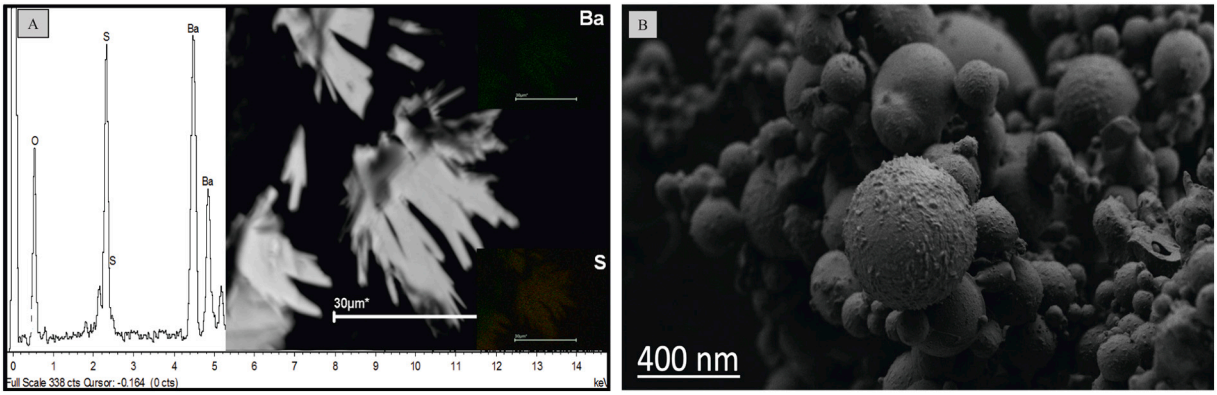


**Fig. 4.** (A) Minerals detected in smaller proportions (e.g. chlorite and illite) and the high presence of fine particles, such as barite; and (B) spherical amorphous phases, similar to coal fly ash, detected in the analyzed particulate material.

whether modern or historic, is also influenced by the air quality in the city of Budapest. This study points to the crucial need for local authorities in Budapest to formulate and implement public policy that actively restores the historical heritage of their UNESCO listed sites.

The analysis of the material collected on the Liberty Bridge, in addition to ultrafine and nanometric carbon particles, also detected the most variable non-organic particles larger than 10 µm. This fact is likely due to the presence of the train that runs on this bridge (Fig. 2,D). Due to its age, its regular operation may be releasing particles containing several toxic elements (Fig. 5) with greater ease of suspension due to wind action or agitation caused by passing vehicles. Fig. 5 shows that while carbon is not inside the particle, it does not prevent particles from interacting with organic phases present in the environment and forming organometallic particles, as reported by Lee (2020), whose study area also included trains.

Fig. 6 illustrates the classic ultra-fine particles containing chemical elements that make up train and meter pellets. As Sb, Cr, Fe and As can be present in rails, pellets and compounds used in transport in trains and meters (Lee, 2020), these elements can be released in that process, thereby increasing human exposure to such elements that are dangerous to human health. Through the areas studied at points A, B, C and D, despite the identification of dangerous elements in ultra-fine particulates, it is necessary to study the patch of atmospheric pollution by satellite, aiming at a better understanding of the dynamics of the patch, and expansion of pollutants over the city of Budapest. According to Plant et al. (2022) the use of satellite images allows analysis in large regions, with more precision of the dynamics of atmospheric contaminants in areas with high urban density.

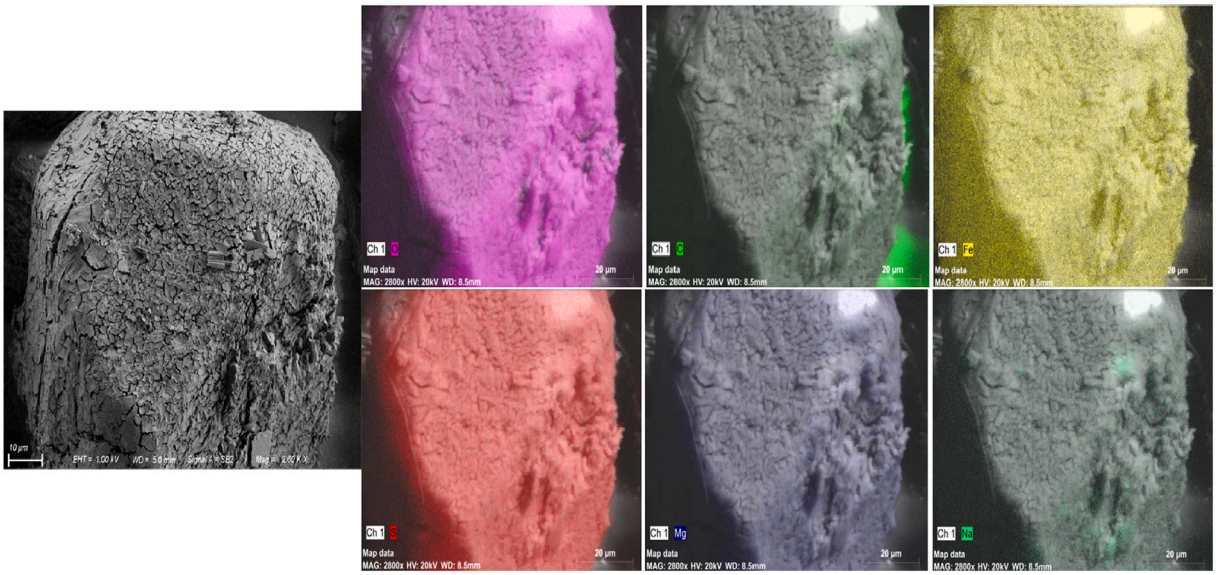


**Fig. 5.** Classic illustrations of barite crystals detected in the samples obtained, almost always particles larger than 10 µm with the presence of ultrafine particles containing several elements toxic to human health, and the durability of buildings and historical monuments.

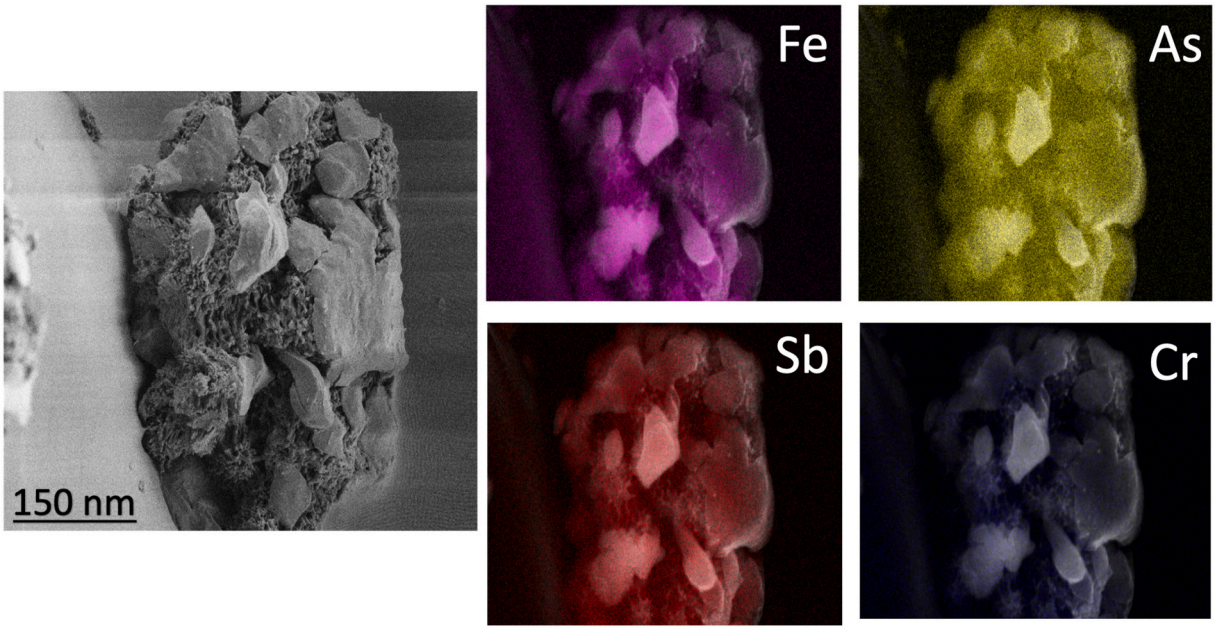


**Fig. 6.** Classic illustrations of ultra-fine particles containing chemical elements Sb, Cr, Fe and As, derived from the composition of train and meter pellets.

### *3.1.1. Potential risks to human health*

Ti, in addition to stimulating the birth of premature babies, can compromise human organs and tissues, causing neurotoxic effects (Ferraro et al., 2020). Even in small proportions, the chemical element V can cause irreversible risks to human health by acting as a carcinogen, leading to the high proliferation of cells of tumorigenic origin (Desaulniers et al., 2021). Guo et al. (2020), when studying the toxicological effects harmful to human health caused by Ni, identified underlying harm related to its immunotoxicity, and Ni may be extremely carcinogenic in the population. When comparing the harmful effects on human health caused by the chemical elements of Ti, V and Ni identified in this study, with other highly relevant research (Ferraro et al., 2020; Guo et al., 2020; Desaulniers et al., 2021), it is highly recommended that the authorities in Budapest create public policies that involve mitigating atmospheric pollution, considering that the current risks of contamination by ultra-fine particles (containing Hg, As, Cd, Pb and other toxic elements) suspended in the air is very real and capable of permanently compromising the quality of urban living.

The presence of the chemical composition of carbonaceous particles smaller than 100 nm was highly diversified, containing

**Table 3**
Major and minor minerals detected in the studied areas.

| Minerals | Area A | Area B | Area C | Area D |
|---|---|---|---|---|
| Albite, $NaAlSiO_8$ | a,c | b,c | a,b,c | a,b,c |
| Anatase, $TiO_2$ | c | c | c | c |
| Aragonite, $CaCO_3$ | b,c | b,c | b,c | b,c |
| Barite, $BaSO_4$ | b,c | b,c | b | c |
| Calcite, $CaCO_3$ | a,b,c | a,b,c | a,b,c | a,b,c |
| Chlorite, $Na_{0.5}Al_6(Si,Al)_8O_{20}(OH)_{10}.H_2O$ | a,b,c | b,c | b,c | a,b,c |
| Dolomite, $CaMg(CO_3)_2$ | b,c | b,c | a,b,c | c |
| Gibbsite, $Al(OH)_3$ | b,c | b,c | b,c | b |
| Gypsum, $Ca[SO_4]\cdot 2H_2O$ | a,b,c | a,b,c | a,b,c | a,b,c |
| K feldspar, $KAlSi_3O_8$ | b,c | c | b,c | b,c |
| Goethite, $Fe(OH)_3$ | b,c | b,c | c | b,c |
| Hematite, $Fe_2O_3$ | b,c | c | b,c | b,c |
| Hexahydrite, $MgSO_4\cdot 6H_2O$ | b,c | b | b | b |
| Illite, $K_{1.5}Al_4(Si_{6.5}Al_{1.5})O_{20}(OH)_4$ | a,b,c | a,b,c | a,b,c | a,b,c |
| Magnetite, | c | c | b,c | c |
| Microcline, $KAlSi_3O_8$ | a,b,c | a,b,c | a,b,c | a,b,c |
| Mullite, $Al_6Si_2O_{13}$ | b,c | a,b,c | b,c | b,c |
| Quartz, $SiO_2$ | a,b,c | a,b,c | a,b,c | a,b,c |
| Rutile, $TiO_2$ | c | c | c | c |

[a] = XDR
[b] = FE-SEM
[c] = HR-TEM

especially dangerous elements such as: silver (Ag), arsenic (As), barium (Ba), carbon (C), cadmium (Cd), chlorine (Cl), cobalt (Co), chromium (Cr), mercury (Hg), germanium (Ge), manganese (Mn), magnesium (Mg), molybdenum (Mo), nickel (Ni), lead (Pb), antimony (Sb), selenium (Se), tin (Sn), strontium (Sr), titanium (Ti), vanadium (V), tungsten (W), zinc (Zn), and zirconium (Zr) (Table 2). Although rare elements such as La, Ce, Th, among others, were not detected, it cannot be ruled out that they are present and may be encapsulated by more abundant phases, or simply were not sampled by the SMPSs. The four studied areas contain a wide variety of nanoparticles with different widths and sizes (Table 3), in addition to containing elements that are highly toxic to human health (Gasparotto et al., 2018; Ferraro et al., 2020; Guo et al., 2020; Desaulniers et al., 2021; Aarzoo and Samim, 2022). Therefore, the suspension of nanoparticles containing hazardous elements is the biggest factor that currently impacts the health of the visiting tourist population. Skalny et al. (2021) and Bao et al. (2022) have demonstrated a high potential for toxicity of As, Hg, Cd, Pb and Cr, which can cause diverse cancers in the population exposed to these atmospheric contaminants.

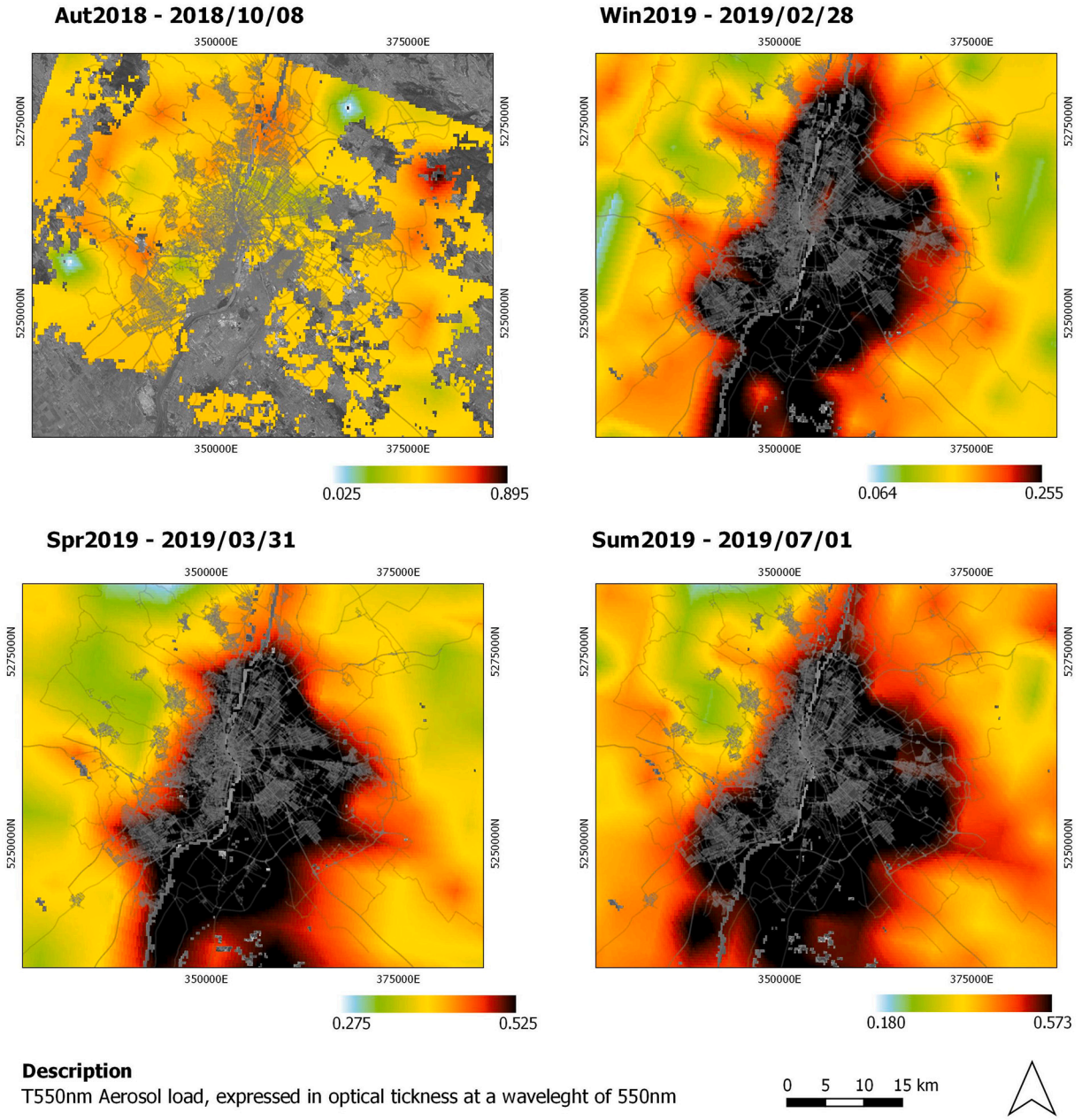


**Fig. 7.** Compositions of images from the Sentinel-3B SYN satellite with representation of the concentrations of Aerosol Optical Thickness (T550) in relation to the following periods: (A) autumn (10/8/2018); (B) winter (2/28/2019); (C) spring (3/31/2019); and (D) summer (7/1/2019).

### 3.2. Assessment of atmospheric contaminants by sentinel-3B SYN satellite images

Through Fig. 7, the compositions provided using Sentinel-3B SYN satellite images were presented to identify the concentration of T550 in the 30 points distributed in the central region and 30 in the peripheral region of Budapest. In Fig. 7, A and C, when demonstrating the analyzed period of autumn ((A) 10/8/2018), and spring ((C) 03/31/2019), lower concentrations of T550 are observed; compared to the winter period ((B) 02/28/2019) and summer ((D) 07/1/2019), where they present values with high concentrations of T550 (Fig. 7, B and D). According to Giannarelli et al. (2019) and Drummond et al. (2022), concentrations of atmospheric contaminants accumulate more in planialtimetric regions with less elevations in altitude, potentiating a high intensity of contaminants at sea level, exposing the population residing in large coastal cities to greater risks of contamination by atmospheric pollutants. This explains the high concentration of T550 identified in the eastern vicinity of the Danube River in Budapest, as it presents lower altitude variation in relation to the other points analyzed by the Sentinel-3B SYN satellite images.

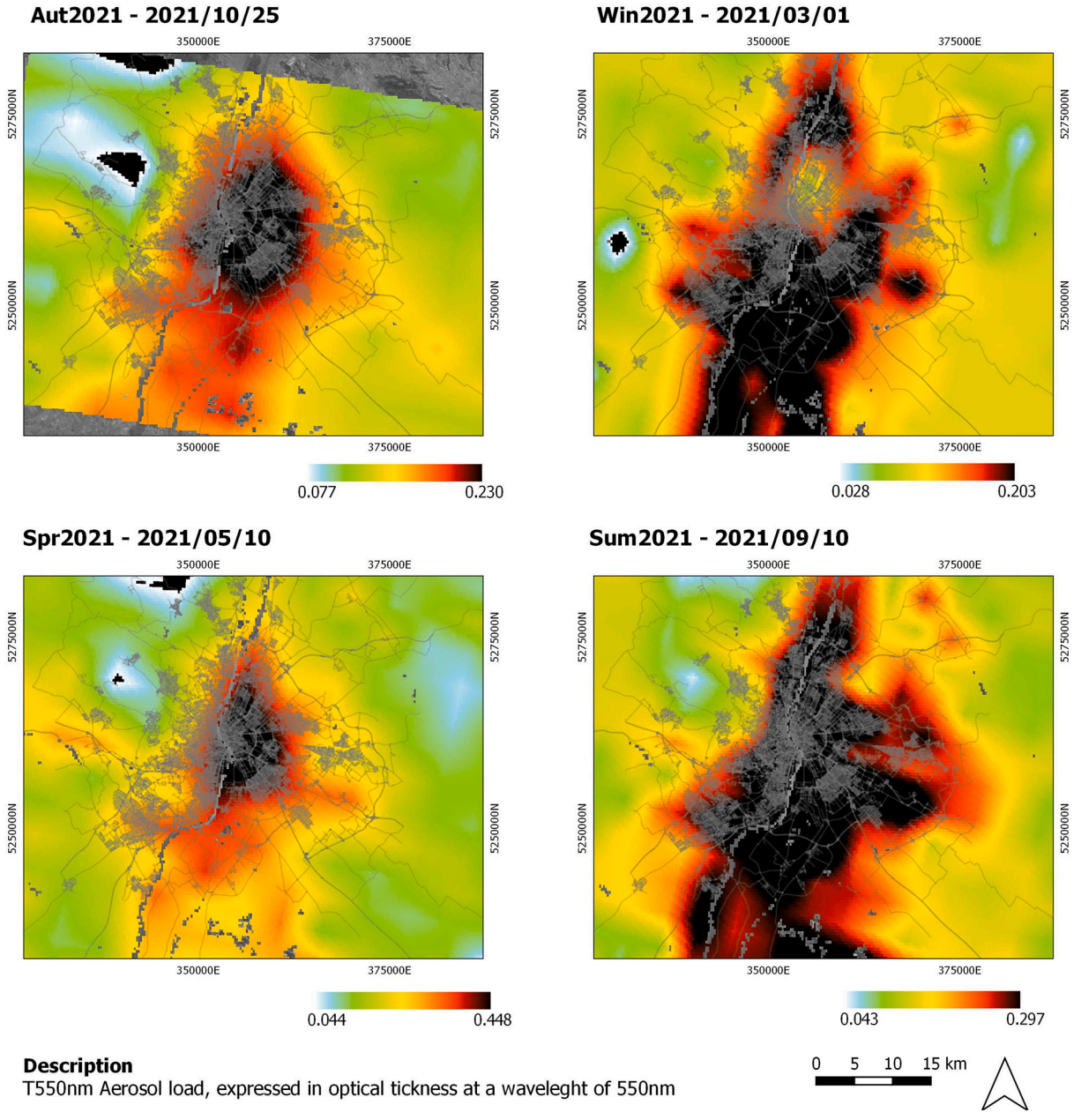


**Fig. 8.** Compositions of images from the Sentinel-3B SYN satellite with representation of Aerosol Optical Thickness (T550) concentrations in relation to the following periods: (A) autumn (10/25/2021); (B) winter (1/3/2021); (C) spring (05/10/2021); and (D) summer (08/10/2021).

Fig. 8 (A, B, C and D) consists of the analysis of the Sentinel-3B SYN satellite images of the year 2021, during the following analysis periods: (A) autumn (10/25/2021), (B) winter (1/03/2021), (C) spring (5/10/2021) and (D) summer (8/10/2021), where it is possible to count a reduction in the concentration of T550 in relation to the analyzed period of 2018 and 2019. This reduction, according to studies by Liu et al. (2021) and Mandal and Patel (2021) is related to the COVID-19 pandemic, which experienced a reduction in atmospheric particles in large global cities. But even in this study, which shows a reduction in the collection of contaminants present in the atmosphere during the analyzed period of 2021, the high presence of T550 in the city of Budapest is still remarkable. Considering that the central area of Budapest has a density of 18.4 inhab/km$^2$, with the highest concentration of T550 in autumn and spring, where the greatest temperature variations occur. Autumn's daily average maximum temperature decreases by 25 °C (from summer) to 6 °C, and spring's maximum daily averages increase from 7 °C (in winter) to 23 °C. It is assumed that the average temperatures in the city of Budapest may be influencing this high dispersion of T550. These results were similar to the studies by Giannarelli et al. (2019) and Drummond et al. (2022), who identified a high presence of atmospheric contaminants related to average temperatures. Figs. 7 and 8 consist of Sentinel-3B SYN images that were used for data collection, through points sampled in Budapest. Figs. 9 and 10 are the results obtained from analysis of Figs. 7 and 8.

The profile of the concentration of T550 identified in 2018 and 2019 (Fig. 9 A), show a high concentration of atmospheric contaminants, with a higher proportion in the city center of Budapest. Another important issue is the role of temperature in the concentration of T550, where higher levels are observed in the summer. These levels decrease as the solar incidence decreases, reaching their lowest levels in the winter. As for the T550 concentration profile in the analyzed period of the year 2021 (Fig. 9 B), the authors wish to highlight the intense urbanization of the area. Large areas of land impervious to water (pavement, structures, etc.) and the use of materials with greater thermal absorption capacity can and does influence the concentration of T550 in Budapest. Again, the COVID-19 pandemic, which occurred during this time, had significant restrictions on the flow of urban mobility. This in turn caused a

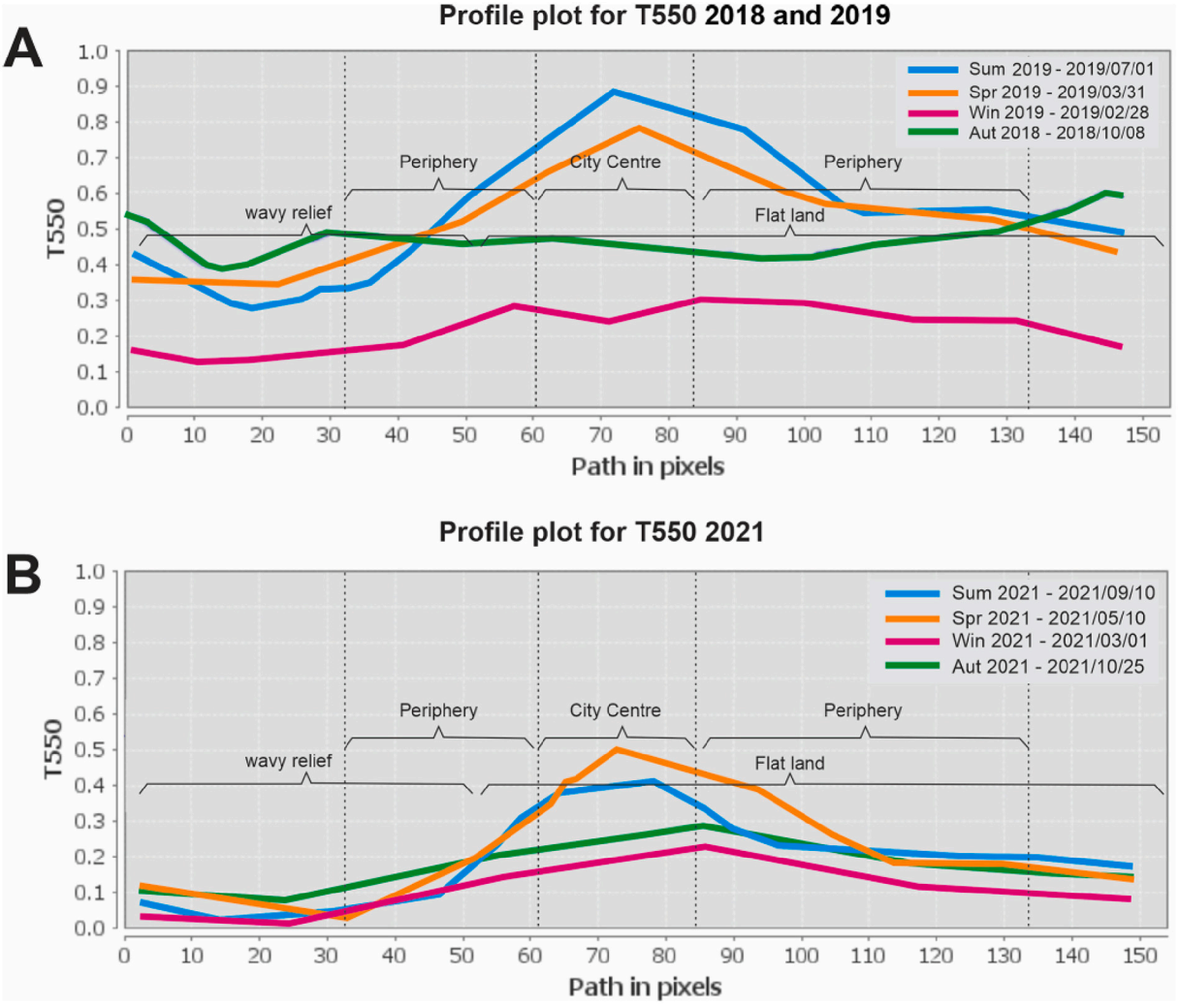


**Fig. 9.** Profile with the variation of Aerosol Optical Thickness (T550) concentrations in relation to the periods analyzed in the years (A) 2018, 2019 and (B) 2021.

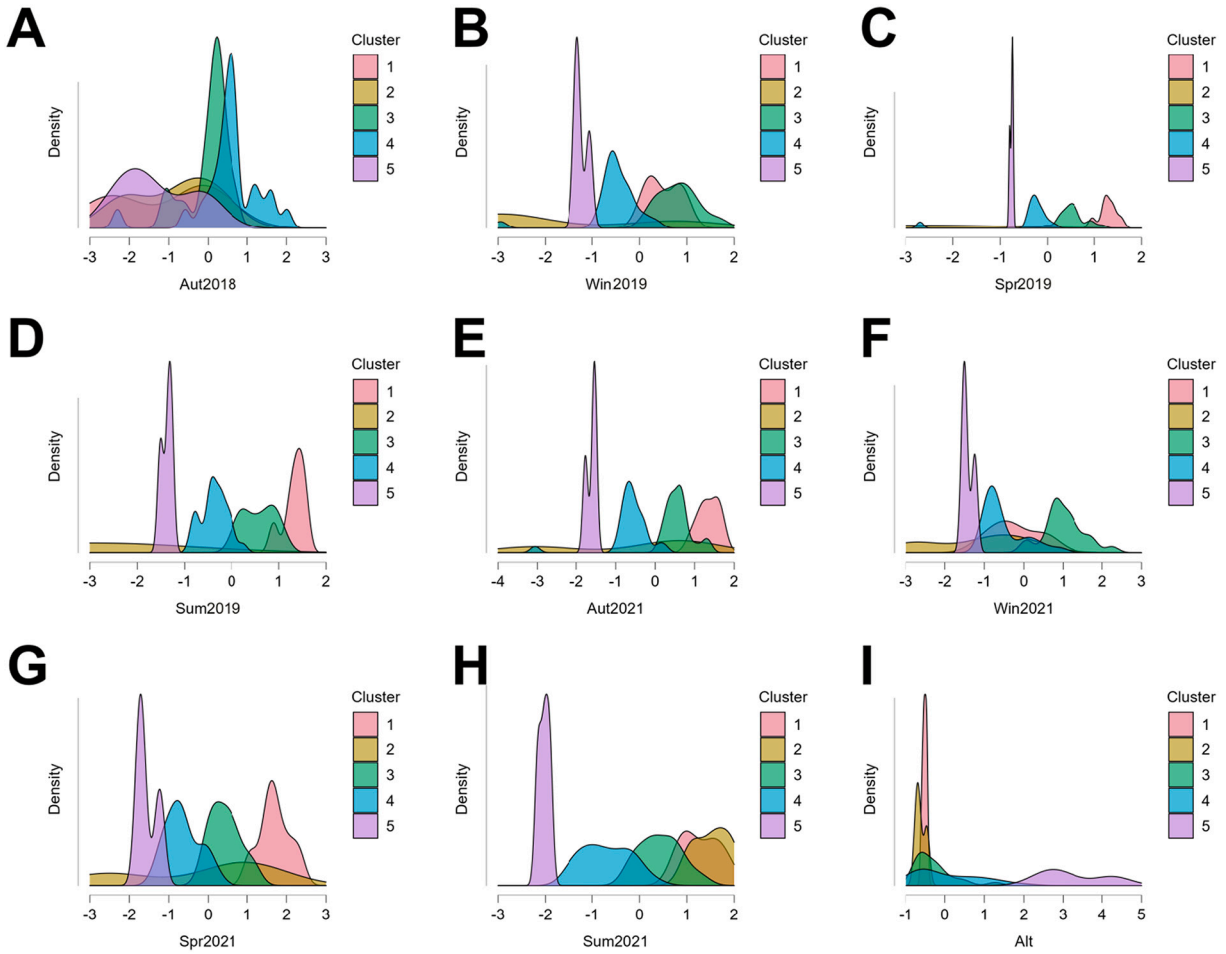


**Fig. 10.** Density graphs, referring to the image compositions of the Sentinel-3B SYN satellite: (A) T550 Aut2018; (B) T550 Win2019; (C) T550 Spr2019; (D) T550 Win2021; (E) T550 Spr2021; (F) T550 Sum2021; (G) T550 Sum2019; (H) T550 Aut2021; (I) Altimetry.

reduction of contaminants released into the atmosphere. Similar results were reported by several authors during the same time frame (Liu et al., 2021; Mandal and Patel, 2021).

It should be noted that the data collected at the points determined in the Sentinel-3B SYN satellite images were subjected to linear statistical description, which allowed a better analysis of T550 concentrations, which were higher in the summers of 2018 and 2019 (Table 4). A clear example presented in this study was that the summer of 2019 presented an average value of 0.556 of T550 in the atmosphere; whereas the summer of 2021 presented a decrease of 0.283 of T550 in the atmosphere. This consists of a T550 reduction of 50.89%, attributed according to Liu et al. (2021) and Mandal and Patel (2021) as a decrease in the emission of air pollutants influenced by the COVID-19 pandemic.

The K-means cluster analysis presented the fit scores for the statistical model, where $K = 5$ clusters for a dataset assigned by the collection points (Tardioli et al., 2018; Naghizadeh and Metaxas, 2020). The observed value of $R^2$ was 0.689, demonstrating that the model presents a good response for this study. The Akaike Information Criterion (AIC) yielded 255,110 and the Bayesian Information Criterion (BIC) was 349,350, proving the quality of fit of a model. However, they penalize the number of free parameters of the model, as models that have a criterion of inferior information are generally perceived with better results (Tardioli et al., 2018; Naghizadeh and Metaxas, 2020). Thus, the silhouette index ranged from zero (0) to one (1), for $K = 5$, the cluster corresponded to 0.36, thus generating a regular trend of clustering, according to the established variables.

The representation of the size of the clusters, with the variability within each cluster, thus considering the sum of squares and the proportion of explained heterogeneity within the cluster and silhouette index was 0.360. As for heterogeneity, the total value of 1 was divided (Naghizadeh and Metaxas, 2020). Cluster 4 is the largest with 25 collection points, and is also the most heterogeneous with a proportion of 0.481, with the other Clusters being heterogeneous (Table 5). Cluster 5 has the lowest sum of squares with 4119, so it can be considered the most homogeneous. In this context, the Silhouette index demonstrates homogeneity and cohesion (Dal Moro et al., 2021). Clusters 1 and 4 present, respectively, with indices of 0.321 and 0.29, demonstrating that there is a good homogeneity between the analyzed clusters (Table 5).

**Table 4**
Descriptive Statistics of the periods analyzed between 2018, 2019 and 2021.

| Descriptive Statistics of the points collected in Budapest | | | | | | | | | |
|---|---|---|---|---|---|---|---|---|---|
| Items | Aut2018 | Win2019 | Spr2019 | Sum2019 | Aut2021 | Win2021 | Spr2021 | Sum2021 | Alt |
| Valid | 60 | 60 | 60 | 60 | 60 | 60 | 60 | 60 | 60 |
| Missing | 0 | 0 | 0 | 0 | 0 | 0 | 0 | 0 | 0 |
| Mean | 0.465 | 0.234 | 0.485 | 0.556 | 0.178 | 0.163 | 0.281 | 0.283 | 190.340 |
| Std. Deviation | 0.052 | 0.079 | 0.180 | 0.191 | 0.058 | 0.059 | 0.111 | 0.096 | 68.052 |
| Minimum | 0.334 | 0.000 | 0.000 | 0.000 | 0.000 | 0.000 | 0.000 | 0.076 | 137.000 |
| Maximum | 0.569 | 0.371 | 0.767 | 0.857 | 0.274 | 0.296 | 0.537 | 0.468 | 480.250 |

**Table 5**
Cluster Information in relation to the points sampled in the Sentinel-3B SYN satellite images collected in the city of Budapest.

| Cluster | 1 | 2 | 3 | 4 | 5 |
|---|---|---|---|---|---|
| Size | 7 | 3 | 22 | 25 | 3 |
| Explained proportion within-cluster heterogeneity | 0.093 | 0.202 | 0.199 | 0.481 | 0.025 |
| Within sum of squares | 15.349 | 33.311 | 32.920 | 79.409 | 4.119 |
| Silhouette score | 0.321 | 0.032 | 0.428 | 0.329 | 0.571 |

Although not strictly part of the k-means clustering technique, it is a useful step when variables have a meaning and an assigned relationship (Dal Moro et al., 2021). Cluster 1 is more influenced by the concentration of T550 in the spring 2021 and autumn 2021 periods, with an index of 1697 and 1351 respectively. The points that make up Cluster 1 are located in the city center of Budapest. There was a greater presence of atmospheric contaminants, identified using the Sentinel-3B SYN satellite images, in addition to confirming the presence of ultra-fine particles and nanoparticles identified by SMPSs (Table 2), capable of causing harmful effects to human health and in historic buildings and monuments.

The concentration of T550 represented in Cluster 2 is influenced by the variables summer 2019, spring 2019 and winter 2019, with an index of 1527, −2688 and − 1707 respectively. Demonstrating that the proximity of the Danube River has an effect on the concentration of T550. The points that make up Cluster 3 are located between the center and the periphery. Cluster 4 has high heterogeneity, it is the largest cluster composed of 25 points. The variable summer 2021 is the highest value, with an index of −0.695. Cluster 5 is highly influenced by altimetry, with an index of 3249, which demonstrates that high relief influences the concentration of T550, since altimetry (Alt) has a low effect on all clusters, showing that there are more determinant issues, such as the urban density in relation to the presence of the Danube River between the seasons of the year during the analyzed period (Fig. 10).

Through Fig. 10, the density graphic of autumn 2018 can be visualized, which considers Clusters 3 and 4, where they represent

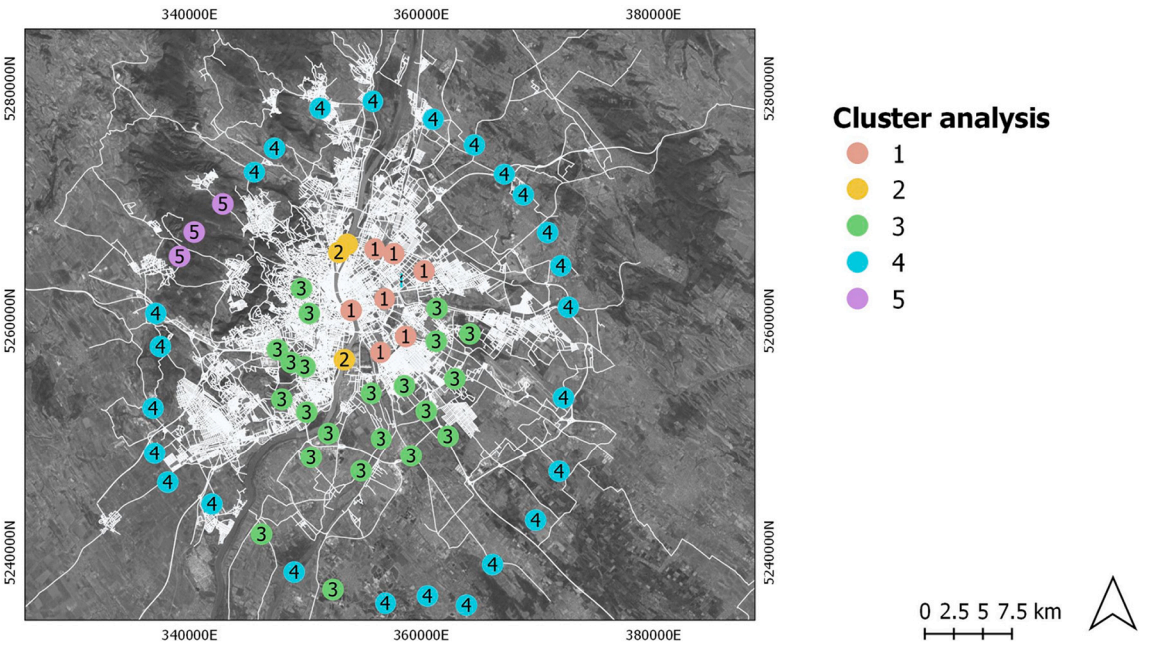


**Fig. 11.** Spatialization map of clusters sampled in the city of Budapest.

peaks in the concentration of T550 (Fig. 10,A). In winter 2019 and winter 2021 (Fig. 10 B and F), Cluster 3 presents higher values in the concentration of T550, higher than cluster 1, a phenomenon that can be explained by the daily thermal amplitude, due to the thermal absorption capacity of the materials present on the terrestrial surface (Neckel et al., 2021). It can be seen in Fig. 10 (C, D, E, G, H) that the variables spring 2019, summer 2019, autumn2021, spring 2021, and summer 2021 form homogeneous clusters. This demonstrates that the concentration of T550 is influenced by the seasons, and by variations in altimetry.

Through Fig. 11 it can be seen that Cluster 1 corresponds to the collection points located in the center of the city, Cluster 2 is located next to the Danube River, Cluster 3 is located in the intermediate zone between the center and the periphery, Cluster 4 is composed of points located on the periphery and Cluster 5 is located in a zone of high terrestrial altimetry. It is possible to understand the dynamics of the variation of atmospheric pollutants with the use of images from the Sentinel-3B SYN satellite compared to the collections obtained by SMPSs containing atmospheric particles of ultra-thin thickness.

## 4. Conclusion

Through the ultra-fine particles collected on SMPSs in the field at the points sampled in the central area of the city of Budapest, it was possible to identify these elements included As, Cd, Cr, Hg, Pb, Ti, V and Ni. Therefore, a contingency plan is suggested for the municipality of Budapest in order to offer greater protection to the health of local residents and visiting tourists, and to better preserve the historical buildings and monuments of the region, given the corrosive degree of these atmospheric pollutants. The Passenger Cruise Port, Kunsthalle, Szechenyi Lanchid, and Liberty Bridge are all listed as UNESCO world heritage sites.

The use of images from the Sentinel-3B SYN satellite demonstrates the abundant presence of T550 in the atmosphere during 2018, 2019 and 2021. Only the year 2021 showed a 50.89% reduction in T550 levels, compared to other analyzed periods. 2018 and 2019 showed worrying levels of atmospheric contaminants in the central areas of Budapest. Through this evidence of the presence of dangerous elements, improvements in urban habitats are suggested, with the elaboration of future studies, capable of creating public policies aimed at mitigating the emission of atmospheric pollutants. Also, studies that quantify the presence of chemical elements is suggested for future studies in the city of Budapest. These studies would make it possible to extrapolate the risks to human health caused by these hazardous elements dispersed in the air to a greater degree.

## Author statement

Alcindo Neckel and Laércio Stolfo Maculan: Conceptualization, Funding acquisition.
Marcos L. S. Oliveira and Brian William Bodah: final manuscript writing.
Affonso Celso Gonçalves Jr. and Luis F. O. Silva: review & editing.

## Declaration of Competing Interest

The authors declare that they have no known competing financial interests or personal relationships that could have appeared to influence the work reported in this paper.

## Data availability

The data that has been used is confidential.

## Acknowledgements

The authors are grateful to the European Space Agency (ESA) and the U.S. National Aeronautics and Space Administration (NASA) for providing the unpublished and treated images originating from the Sentinel-3B SYN satellite. The NOAA Air Resources Laboratory (ARL) for the provision of the HYSPLIT transport and dispersion model and/or READY website (http://www.ready.noaa.gov) used in this publication. We also wish to thank the National Council for Scientific and Technological Development (CNPq), Brazil.

## References

Aarzoo, N., Samim, M., 2022. Palladium nanoparticles as emerging pollutants from motor vehicles: an in-depth review on distribution, uptake and toxicological effects in occupational and living environment. Sci. Total Environ. 823, 153787 https://doi.org/10.1016/j.scitotenv.2022.153787.

Addington, O., Zeng, Z.C., Pongetti, T., Shia, R.L., Gurney, K.R., Liang, J., Roest, G., He, L., Yung, Y.L., Sander, S.P., 2021. Estimating nitrous oxide ($N_2O$) emissions for the Los Angeles Megacity using mountaintop remote sensing observations. Remote Sens. Environ. 259, 112351 https://doi.org/10.1016/j.rse.2021.112351.

Bao, J., Li, H., Wu, Z., Zhang, X., Zhang, H., Li, Y., Qian, J., Chen, J., Deng, L., 2022. Atmospheric carbonyls in a heavy ozone pollution episode at a metropolis in Southwest China: characteristics, health risk assessment, sources analysis. Res. J. Environ. Sci. 113, 40–54. https://doi.org/10.1016/j.jes.2021.05.029.

Bodah, B.W., Neckel, A., Stolfo Maculan, L., Milanes, C.B., Korcelski, C., Ramírez, O., Mendez-Espinosa, J.F., Bodah, E.T., Oliveira, M.L., 2022. Sentinel-5P TROPOMI satellite application for $NO_2$ and CO studies aiming at environmental valuation. J. Clean. Prod. 357, 131960 https://doi.org/10.1016/j.jclepro.2022.131960.

Buzási, A., 2022. Comparative assessment of heatwave vulnerability factors for the districts of Budapest, Hungary. Urban Clim. 42, 101127 https://doi.org/10.1016/j.uclim.2022.101127.

Buzási, A., Pálvölgyi, T., Csete, M.S., 2021. Assessment of climate change performance of urban development projects – case of Budapest, Hungary. Cities 114, 103215. https://doi.org/10.1016/j.cities.2021.103215.

Dai, S., Finkelman, R.B., French, D., Hower, J.C., Graham, I.T., Zhao, F., 2021. Modes of occurrence of elements in coal: a critical evaluation. Earth-Sci. Rev. 222, 103815 https://doi.org/10.1016/j.earscirev.2021.103815.

Dal Moro, L., Maculan, L.S., Neckel, A., De Vargas Mores, G., Pivoto, D., Bodah, E.T., Bodah, B.W., Oliveira, M.L., 2021. Geotechnologies applied to the analysis of buildings involved in the production of poultry and swine to the integrated food safety system and environment. J. Environ. Chem. Eng. 9 (6), 106475 https://doi.org/10.1016/j.jece.2021.106475.

Desaulniers, D., Cummings-Lorbetskie, C., Leingartner, K., Xiao, G.H., Zhou, G., Parfett, C., 2021. Effects of vanadium (sodium metavanadate) and aflatoxin-B1 on cytochrome p450 activities, DNA damage and DNA methylation in human liver cell lines. Toxicol. in Vitro 70, 105036. https://doi.org/10.1016/j.tiv.2020.105036.

Dong, Y., Yuan, H., Bai, L., Ge, D., Zhu, N., 2021. A comprehensive study on simultaneous enhancement of sludge dewaterability and elimination of polycyclic aromatic hydrocarbons by $Fe^{2+}$ catalyzing $O_3$ process. Sci. Total Environ. 152015 https://doi.org/10.1016/j.scitotenv.2021.152015.

Dövényi, Z., Kovács, Z., Kincses, Á., Bálint, L., Egedy, T., 2021. Migration. In: Kocsis, K. (Editor-in-Chief): National Atlas of Hungary – *Society*. Budapest, CSFK Geographical Institute, pp. 44–57.

Drummond, L.D.O., Meire, R.O., Braga, C., Rezende, C.E.D., Malm, O., Cerqueira, R., 2022. Trophic position, altitudinal distribution, and water dependence as determining factors for mercury concentrations in tropical montane anurans. Sci. Total Environ. 806, 151356 https://doi.org/10.1016/j.scitotenv.2021.151356.

ESA (European Space Agency), 2022. Sentinel-5P Pre-Operations Data Hub - European. https://s5phub.copernicus.eu/dhus/.

Fernandez-Moran, R., Gómez-Chova, L., Alonso, L., Mateo-García, G., López-Puigdollers, D., 2021. Towards a novel approach for Sentinel-3 synergistic OLCI/SLSTR cloud and cloud shadow detection based on stereo cloud-top height estimation. ISPRS J. Photogramm. Remote Sens. 181, 238–253. https://doi.org/10.1016/j.isprsjprs.2021.09.013.

Ferraro, S.A., Domingo, M.G., Etcheverrito, A., Olmedo, D.G., Tasat, D.R., 2020. Neurotoxicity mediated by oxidative stress caused by titanium dioxide nanoparticles in human neuroblastoma (SH-SY5Y) cells. J. Trace Elem. Med. Biol. 57, 126413 https://doi.org/10.1016/j.jtemb.2019.126413.

Forest, V., 2021. Combined effects of nanoparticles and other environmental contaminants on human health - an issue often overlooked. Nanoimpact 23, 100344. https://doi.org/10.1016/j.impact.2021.100344.

García, D.H., Díaz, J.A., 2022. Impacts of the COVID-19 confinement on air quality, the land surface temperature and the urban heat island in eight cities of Andalusia (Spain). Remote Sens. Appl.: Soc. Environ. 25, 100667 https://doi.org/10.1016/j.rsase.2021.100667.

García-Florentino, C., Maguregui, M., Carrero, J.A., Morillas, H., Arana, G., Madariaga, J.M., 2020. Development of a cost effective passive sampler to quantify the particulate matter depositions on building materials over time. J. Clean. Prod. 268, 122134 https://doi.org/10.1016/j.jclepro.2020.122134.

Gasparotto, J., Chaves, P.R., da Boit Martinello, K., da Rosa-Siva, H.T., Bortolin, R.C., Nordin, A.P., Soares, K., Borges, M.S., Gelain, D.P., Moreira, J.C.F., 2018. Obese rats are more vulnerable to inflammation, genotoxicity and oxidative stress induced by coal dust inhalation than non-obese rats. Ecotoxicol. Environ. Saf. 165, 44–51. https://doi.org/10.1016/j.ecoenv.2018.08.097.

Giannarelli, S., Onor, M., Abete, C., Termine, M., Fuoco, R., 2019. Effect of altitude and distance from the sea on fractionation processes of Persistent Organic Pollutants (POPs) associated to atmospheric aerosol from Ross Sea to Dome C, Antarctica. Microchem. J. 149, 103911 https://doi.org/10.1016/j.microc.2019.05.012.

Guo, H., Liu, H., Jian, Z., Cui, H., Fang, J., Zuo, Z., Deng, J., Li, Y., Wang, X., Zhao, L., He, R., Tang, H., 2020. Immunotoxicity of nickel: pathological and toxicological effects. Ecotoxicol. Environ. Saf. 203, 111006 https://doi.org/10.1016/j.ecoenv.2020.111006.

IAMAT - International Association for Mediacal Assistance to Travellers, 2022. Hungary General Health Risks: Air Pollution. https://www.iamat.org/country/hungary/risk/air-pollution#:~:text=The%20most%20recent%20data%20indicates,mining%20industry%2C%20and%20vehicle%20emissions (Accessed 18 January 2022).

Islam, N., Dihingia, A., Khare, P., Saikia, B.K., 2020. Atmospheric particulate matters in an Indian urban area: health implications from potentially hazardous elements, cytotoxicity, and genotoxicity studies. J. Hazard. Mater. 384, 121472 https://doi.org/10.1016/j.jhazmat.2019.121472.

Kong, Y., Ma, N.L., Yang, X., Lai, Y., Feng, Z., Shao, X., Xu, X., Zhang, D., 2020. Examining $CO_2$ and $N_2O$ pollution and reduction from forestry application of pure and mixture forest. Environ. Pollut. 265, 114951 https://doi.org/10.1016/j.envpol.2020.114951.

Kovács, Z., Farkas, Z.J., Egedy, T., Kondor, A.C., Szabó, B., Lennert, J., Baka, D., Kohán, B., 2019. Urban sprawl and land conversion in post-socialist cities: the case of metropolitan Budapest. Cities 92, 71–81. https://doi.org/10.1016/j.cities.2019.03.018.

Kovács, A., Leelőssy, D., Tettamanti, T., Esztergár-Kiss, D., Mészáros, R., Lagzi, I., 2021. Coupling traffic originated urban air pollution estimation with an atmospheric chemistry model. Urban Clim. 37, 100868 https://doi.org/10.1016/j.uclim.2021.100868.

Lee, H., 2020. Generation characteristics of the airborne wear particles emitted from the wheel-rail contact for various train velocities and their generation relation with the train velocity. Atmos. Environ. 5, 100068 https://doi.org/10.1016/j.aeaoa.2020.100068.

Li, F., Hu, G., Li, S., Hou, C., Gao, J., 2020. Dual-confined sulfur cathodes based on $SnO_2$-decorated $MoS_2$ microboxes for long-life lithium–sulfur batteries. Electrochim. Acta 340, 135991. https://doi.org/10.1016/j.electacta.2020.135991.

Li, M., Liu, W., Liu, W., Bi, M., Cui, Z., 2021. Dynamic substance flow analysis of lead in the fossil fuel system of China from 1980 to 2018. J. Clean. Prod. 313, 127918 https://doi.org/10.1016/j.jclepro.2021.127918.

Li, S., Chen, F., Song, K., Liu, G., Tao, H., Xu, S., Wang, X., Wang, Q., Mu, G., 2022. Mapping the trophic state index of Eastern Lakes in China using an empirical model and sentinel-2 imagery data. J. Hydrol. 127613 https://doi.org/10.1016/j.jhydrol.2022.127613.

Liu, L., Lin, Q., Liang, Z., Du, R., Zhang, G., Zhu, Y., Qi, B., Zhou, S., Li, W., 2021. Variations in concentration and solubility of iron in atmospheric fine particles during the COVID-19 pandemic: an example from China. Gondwana Res. 97, 138–144. https://doi.org/10.1016/j.gr.2021.05.022.

Mandal, J., Patel, P.P., 2021. Gauging the effects of the COVID-19 pandemic lockdowns on atmospheric pollution content in select countries. Remote Sens. Appl.: Soc. Environ. 23, 100551 https://doi.org/10.1016/j.rsase.2021.100551.

Marvila, M.T., Azevedo, A.R., Barroso, L.S., Barbosa, M.Z., De Brito, J., 2020. Gypsum plaster using rock waste: a proposal to repair the renderings of historical buildings in Brazil. Constr. Build. Mater. 250, 118786 https://doi.org/10.1016/j.conbuildmat.2020.118786.

Mei, L., Rozanov, V., Burrows, J.P., 2020. A fast and accurate radiative transfer model for aerosol remote sensing. J. Quant. Spectrosc. Radiat. Transf. 256, 107270 https://doi.org/10.1016/j.jqsrt.2020.107270.

Morillas, H., García-Florentino, C., Marcaida, I., Maguregui, M., Arana, G., Silva, L.F., Madariaga, J.M., 2018. In-situ analytical study of bricks exposed to marine environment using hand-held X-ray fluorescence spectrometry and related laboratory techniques. Spectrochim. Acta B At. Spectrosc. 146, 28–35. https://doi.org/10.1016/j.sab.2018.04.020.

Murukutti, M.K., Jena, H., 2022. Synthesis of nano-crystalline zeolite-A and zeolite-X from Indian coal fly ash, its characterization and performance evaluation for the removal of $Cs^+$ and $Sr^{2+}$ from simulated nuclear waste. J. Hazard. Mater. 423, 127085 https://doi.org/10.1016/j.jhazmat.2021.127085.

Naghizadeh, A., Metaxas, D.N., 2020. Condensed silhouette: an optimized filtering process for cluster selection in K-means. Proc. Comput. Sci. 176, 205–214. https://doi.org/10.1016/j.procs.2020.08.022.

Nassajpour-Esfahani, A.H., Alhaji, A., Hahftbaradaran-Esfahani, M.R., Emadi, R., Bahrami, A., 2021. Oxidation and phase transformation behaviors of $Si_3N_4$-$xMgAl_{12}O_4$ ($0 < x < 90$ wt.%) nanocomposites in vacuum, air, and nitrogen atmospheres. Ceram. Int. 47 (21), 30807–30814. https://doi.org/10.1016/j.ceramint.2021.07.261.

Neckel, A., Oliveira, M.L., Castro Bolaño, L.J., Maculan, L.S., Moro, L.D., Bodah, E.T., Moreno-Ríos, A.L., Bodah, B.W., Silva, L.F., 2021. Biophysical matter in a marine estuary identified by the Sentinel-3B OLCI satellite and the presence of terrestrial iron (Fe) nanoparticles. Mar. Pollut. Bull. 173, 112925 https://doi.org/10.1016/j.marpolbul.2021.112925.

Ngah Nasaruddin, A., Tee, B.T., Mohd Tahir, M., Md Jasman, M.E.S., 2021. Data assessment on the relationship between typical weather data and electricity consumption of academic building in Melaka. Data Br. 35, 106797 https://doi.org/10.1016/j.dib.2021.106797.

Oliveira, M.L., Neckel, A., Pinto, D., Maculan, L.S., Dotto, G.L., Silva, L.F., 2021. The impact of air pollutants on the degradation of two historic buildings in Bordeaux, France. Urban Clim. 39, 100927 https://doi.org/10.1016/j.uclim.2021.100927.

Pinto, D., Neckel, A., Dotto, G.L., Adelodun, B., 2021. Indoor nanoparticle characterization in construction waste recycling companies over time. Sustainability 13 (24), 14071. https://doi.org/10.3390/su132414071.

Pirmana, V., Alisjahbana, A.S., Yusuf, A.A., Hoekstra, R., Tukker, A., 2021. Environmental costs assessment for improved environmental-economic account for Indonesia. J. Clean. Prod. 280, 124521 https://doi.org/10.1016/j.jclepro.2020.124521.

Plant, G., Kort, E.A., Murray, L.T., Maasakkers, J.D., Aben, I., 2022. Evaluating urban methane emissions from space using TROPOMI methane and carbon monoxide observations. Remote Sens. Environ. 268, 112756 https://doi.org/10.1016/j.rse.2021.112756.

Sánchez, J.S., Romaní, J.V., Alves, C., 2011. Deposition of particles on gypsum-rich coatings of historic buildings in urban and rural environments. Constr. Build. Mater. 25 (2), 813–822. https://doi.org/10.1016/j.conbuildmat.2010.07.001.

Silva, L.F., Oliveira, M.L., Neckel, A., Maculan, L.S., Milanes, C.B., Bodah, B.W., Cambrussi, L.P., Dotto, G.L., 2022. Effects of atmospheric pollutants on human health and deterioration of medieval historical architecture (North Africa, Tunisia). Urban Clim. 41, 101046 https://doi.org/10.1016/j.uclim.2021.101046.

Skalny, A.V., Aschner, M., Bobrovnitsky, I.P., Chen, P., Tsatsakis, A., Paoliello, M.M., Buha Djordevic, A., Tinkov, A.A., 2021. Environmental and health hazards of military metal pollution. Environ. Res. 201, 111568 https://doi.org/10.1016/j.envres.2021.111568.

Tardioli, G., Kerrigan, R., Oates, M., O'Donnell, J., Finn, D.P., 2018. Identification of representative buildings and building groups in urban datasets using a novel pre-processing, classification, clustering and predictive modelling approach. Build. Environ. 140, 90–106. https://doi.org/10.1016/j.buildenv.2018.05.035.

Zhang, H., Ji, Y., Wu, Z., Peng, L., Bao, J., Peng, Z., Li, H., 2022. Atmospheric volatile halogenated hydrocarbons in air pollution episodes in an urban area of Beijing: characterization, health risk assessment and sources apportionment. Sci. Total Environ. 806, 150283 https://doi.org/10.1016/j.scitotenv.2021.150283.